Received: 28 January 2021 | Revised: 25 April 2021 | Accepted: 16 May 2021

DOI: 10.1002/nano.202100043

RESEARCH ARTICLE

Nano Select Open Access WILEY

Adhesion and proliferation of living cell on surface functionalized with glycine nanostructures

Aminur Rahman[1] | **Kumar Jyotirmoy Roy**[1] | **K. M. Ashikur Rahman**[2] | **Mst. Khudishta Aktar**[1] | **Md. Abdul Kafi**[1] | **Md. Shafiqul Islam**[1] | **Md. Bahanur Rahman**[1] | **Md. Rafiqul Islam**[3] | **Khandker Saadat Hossain**[2] | **Md. Mizanur Rahman**[2] | **Hadi Heidari**[4]

[1] Department of Microbiology and Hygiene, Bangladesh Agricultural University, Mymensingh, Bangladesh

[2] Department of Physics, University of Dhaka, Dhaka, Bangladesh

[3] Bangladesh Agricultural Research Council, Farm gate, Dhaka, Bangladesh

[4] James Watt School of Engineering, University of Glasgow, Glasgow, UK

Correspondence
Md. Abdul Kafi, Department of Microbiology and Hygiene, Bangladesh Agricultural University, Mymensingh 2202, Bangladesh.
Email: makafi2003@bau.edu.bd

Funding information
Ministry of Education; Banbeis, Grant/Award Number: LS2018687; International Science Program

Abstract

This research presents the application of glycine amino acid for establishing firm cell-substrate interaction instead of expensive adhesion proteins, peptides and peptide derivatives. The glycine amino acid is chemically functionalized on the coverslip to achieve self-assembled nanostructure. Glycine self-assembly on NaCl treated coverslips is initiated with $SiONa^{+}$:COO^{-} linkage while their nanostructure is achieved with formation of glycine chain through NH_3^{+}:COO^{-} covalent linkage between the adjacent molecules. The functionalization steps are confirmed by Fourier-transform infrared spectroscopy (FTIR) investigation. The atomic force microscopy (AFM) and scanning electron microscopy (SEM) investigations reveal that glycine growth initiates at 4 Hours (H) post-treatment while maximum growth appears after 8H-10H. Both the vertical and horizontal growth of nanostructures show dependence on functionalization periods. Various levels of glycine functionalized surface show different levels of baby hamster kidney (BHK-21) cell adhesion and proliferation efficiency with maximum performance for 10H functionalized surface. The adhesion and proliferation performance of 10H glycine functionalized surface shows negligible difference when compared with glycine-aspartic acid (RGD) functionalized surface. Finally, growth curves obtained from both glycine and RGD functionalized surface reveal exponential growth phage up to 48H followed by stationary phage between 48H and 72H while death of many cells appears from 72H to 96H. Thus, this research concluded that glycine functionalized surface is equally effective for cell adhesion and proliferation.

KEYWORDS
adhesion, adhesion molecules, BHK-21 cell, cell-substrate, glycine, proliferation

1 | INTRODUCTION

The cell-substrate interaction studies have attracted much attention in many fields of cell biology, tissue engineering, biomedical sciences, environmental monitoring, pharmacology, basic neuroscience and toxicology.[1,2] Generally, cell-substrate interaction is largely dependent on substrate's biocompatibility, adhesion receptor's availability and other biophysical conditions such as cell health, nutrient availability, pH, Tm, humidity and so on. Among these essential elements of cell-substrate interaction studies, the availability of adhesion molecules (AM)[2,3] and their nano-structural organization[4] on substrate possess significant impact. Basically, cells at in vivo condition remain attached with extracellular matrix protein (ECM) through numerous AM such as Fibronectin, Collagen, Laminin, poly-L-lysine, Arginine-Glycine-Aspartic Acid (RGD) peptides, and so on.[5] Hence, immobilization of cells at in vitro requires functionalization of artificial surfaces with those AMs. Several previous studies focused on the cell-substrate interface for establishing firm interaction through nanoscale engineering of AMs to improve cell adhesion and proliferation.[6] At the beginning of such approaches, many researchers employed entire ECM component for enhancing cell adhesion ability of artificial surface.[7] Later, it was reported that major portions of ECM component do not involve in the adhesion process since only specific fibers of ECM such as fibronectin, vitronectin, laminin, and so on, offered specific region/motif for cell adhesion process.[8–10] It was also reported that instead of whole fiber, the only specific regions of amino acid sequences of fibronectin, laminin, and collagen are involved in the cell attachment process.[10,11] Therefore, as an alternate of bulk ECM materials many peptide sequences from their adhesion motifs such as RGD, Isoleucine-Lysine-Valine-Alanine-Valine (IKVAV), Tyrosine-Isoleucine-Glycine-Serine-Arginine (YIGSR), Aspartic-Glycine-Glutamic-Alanine (DGEA), and so on. were investigated for evaluating cell adhesion ability.[12–15] Among these peptide sequences maximum cell adhesion was reported with RGD peptide while poor adhesion was achieved using IKVAV, YIGSR, and PRARI peptides respectively.[16,17] Likewise, several polymers tagged peptide hybrid structures such as polyurethanes (PEU), PEU-COOH, PEU-GRGESY, PEU-GRGDVY, and PEUGRGDSY were also evaluated for cell adhesion purpose.[18] Among these hybrid structures, maximum adhesion was reported from PEU-GRGDVY and PEUGRGDSY because of the presence of RGD in their backbone.[4,19] In an another study, significant improvement of cell adhesion was reported from RGD-peptide coated polytetrafluoroethylene (ePTFE) grafts, while poor adhesion was reported when fibronectin was employed.[20] Based on these proven adhesion abilities, the RGD tripeptide sequence has attracted much attention in many tissue engineering, cell-on-chip and lab-on-chip applications for establishing cells on artificial surfaces.[21–22] Additionally, many researchers also investigated cell adhesion ability of several derivatives of synthetic RGD peptides such as $C(RGD)_4$, RGD-MAP-C and PLL-RGD and so on.[23,24] The cell adhesion showed dependence on various arrangements amino acid residue of those peptides as well as their nano-structural topographic arrangement on artificial surfaces.[25] However, applications of such synthetic RGD and RGD derivatives are expensive because of their intricate designing, synthesis and purification process.[26] Therefore, researchers are still exploring cost-effective cell adhesion motif for establishing firm adhesion strength at cell-substrate interfaces for Tissue engineering, Cell-on-chip and Lab-on-chip applications.

Further investigation on adhesion domains of types I, II, III, IV, and XI collagen[27–29] revealed a chain of primarily repeating [Gly-X- Y] triplets,[30,31] where X and Y was Pro, Hyp, Arg, Asp, and so on, such as $(Pro\text{-}Pro\text{-}Gly)_{8,}$ (Gluv-Pro-Arg-Gly-Asp-Thr) or $(Pro\text{-}Hyp\text{-}Gly)_8$,[32] with various integrity ratio of the amino acid were maximum for Gly (40%) compared with Pro (25.8%), Hyp (25.8%), Asx (6.4%), Ala (3.2%), Val (2.8%), Tyr (1.3%), Lys (8.8%), and Alanine-Histidine-Alanine(3.4%).[33] Thus, glycine was found to be the most abundant component for cell adhesion motif and their biochemical features were further investigated for determining potential cell adhesion ability.[2] Differently from this, it was also reported that a peptide sequence that contains an acidic amino acid-rich region(s) showed improved cell adhesion ability.[34] In this context, among the three amino acid residues of the RGD peptides, Glycine (G = 2.34 pKa) is more acidic than Arginine (D = 12.5 pKa), and Aspartic acid (D = 3.9 pKa),[35] supporting that glycine could be the potential amino acid responsible for cell adhesion. Additionally, among the three amino acid residues of the RGD tri-peptide sequence, only Glycine (G) is hydrophilic while Arginine (R) and Aspartic acid (D) are hydrophobic.[36] These bio physicochemical features of amino acid residues supported that the adhesion potential of RGD peptide sequences might be due to the glycine residue in their backbone. However, such hypothesis of the adhesion potential of glycine amino acid has to be explored further through in vitro cell adhesion and proliferation studies.

Herein, to test this hypothesis, only glycine amino acid was functionalized on a coverslip with the aim of enhancing cell adhesion and proliferation efficiency. The whole research was performed through accomplishing three necessary steps (Figure 1) such as (i) glycine functionalization, (ii) physical characterizations of functionalization

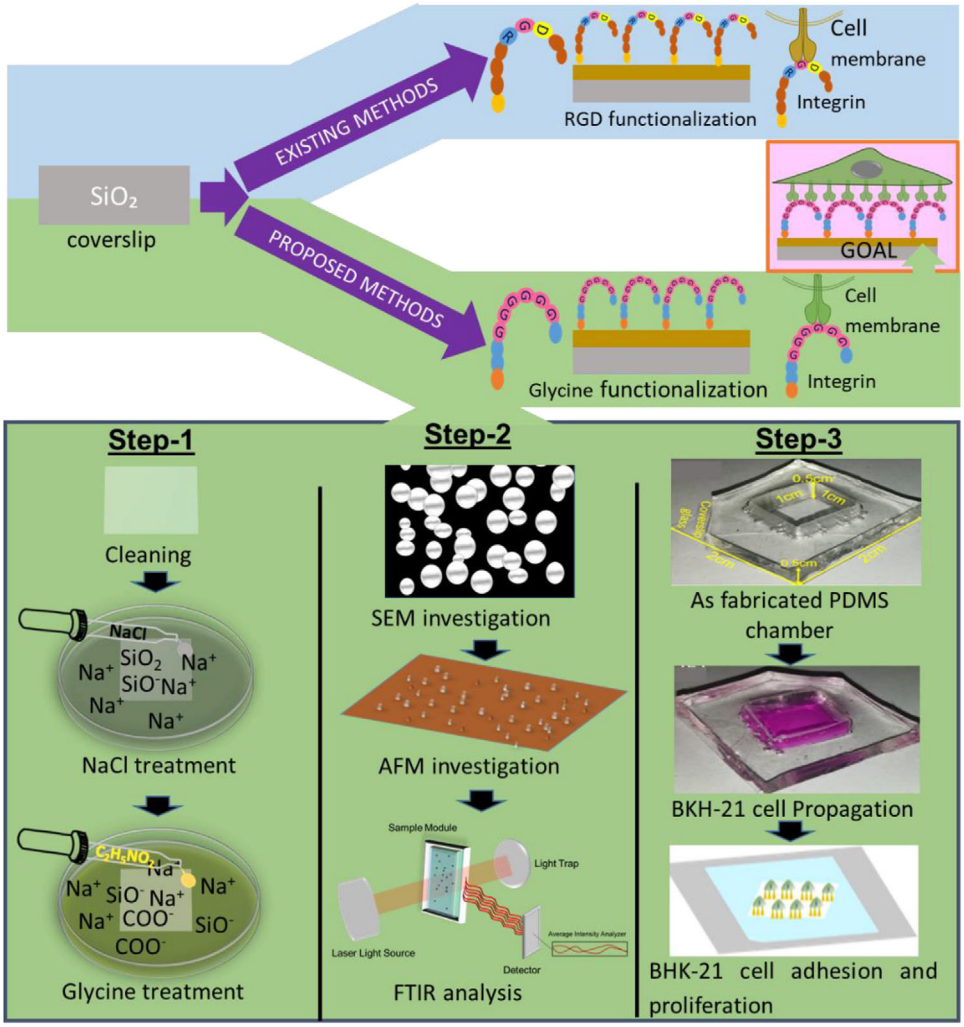

FIGURE 1 Schematic illustrations of living cell adhesion and proliferation on glycine functionalized coverslip: (top) existing procedures of RGD peptide functionalization, (down) the proposed glycine functionalization methods which will be performed step-by-step: Step-1, showed the functionalization process of glycine on coverslip; Step-2, topographic investigation of functionalization surfaces using SEM, AFM, and FTIR; Step-3, shows the living cell adhesion and proliferation using glycine functionalization surface

steps and (iii) cell adhesion and proliferation assay on the functionalized surface. The glycine functionalization was initiated by establishing SiONa group[37] on a freshly cleaned coverslip, which was later act as anchoring site for glycine through establishing $SiONa^+$:COO^- covalent linkage[28,39] and thus initiates self-assembly of glycine on coverslip while their vertical growth was achieved with NH_3^+:COO^- linkage[40] of two adjacent glycine molecules. Fourier-transform infrared spectroscopy (FTIR), atomic force microscopy (AFM), and scanning electron microscopy (SEM) investigations of each functionalization steps were performed for confirming the glycine functionalization process. Finally, the glycine functionalized surface was subjected to in vitro Baby Hamster Kidney (BHK-21) cell adhesion and proliferation assay for unveiling the adhesion efficiencies of glycine amino acids.

2 | RESULTS AND DISCUSSION

Glycine, a commonly available amino acid residue in the backbone of most AMs were nanostructured on a coverslip for enhancing efficiencies of BHK-21 cell adhesion and proliferation. This was achieved with self-assembling of glycine amino acid on Na^+ ionized coverslip where COO^- group of glycine established covalent linkage with the Na^+ forming COONa (Figure 2).[38,39] The Na^+ ionized coverslip was achieved with the treatment of NaCl on the freshly cleaned coverslip. Later, glycine growth occurred through the zwitterion[41] form of NH_3^+ group of glycine that covalently linked with the COO^- group of adjacent glycine molecule for establishing NH_3^+:OOC^- linkage[42] and thus vertical growth of glycine nanostructures occurred. These self-assembled glycine nanostructures

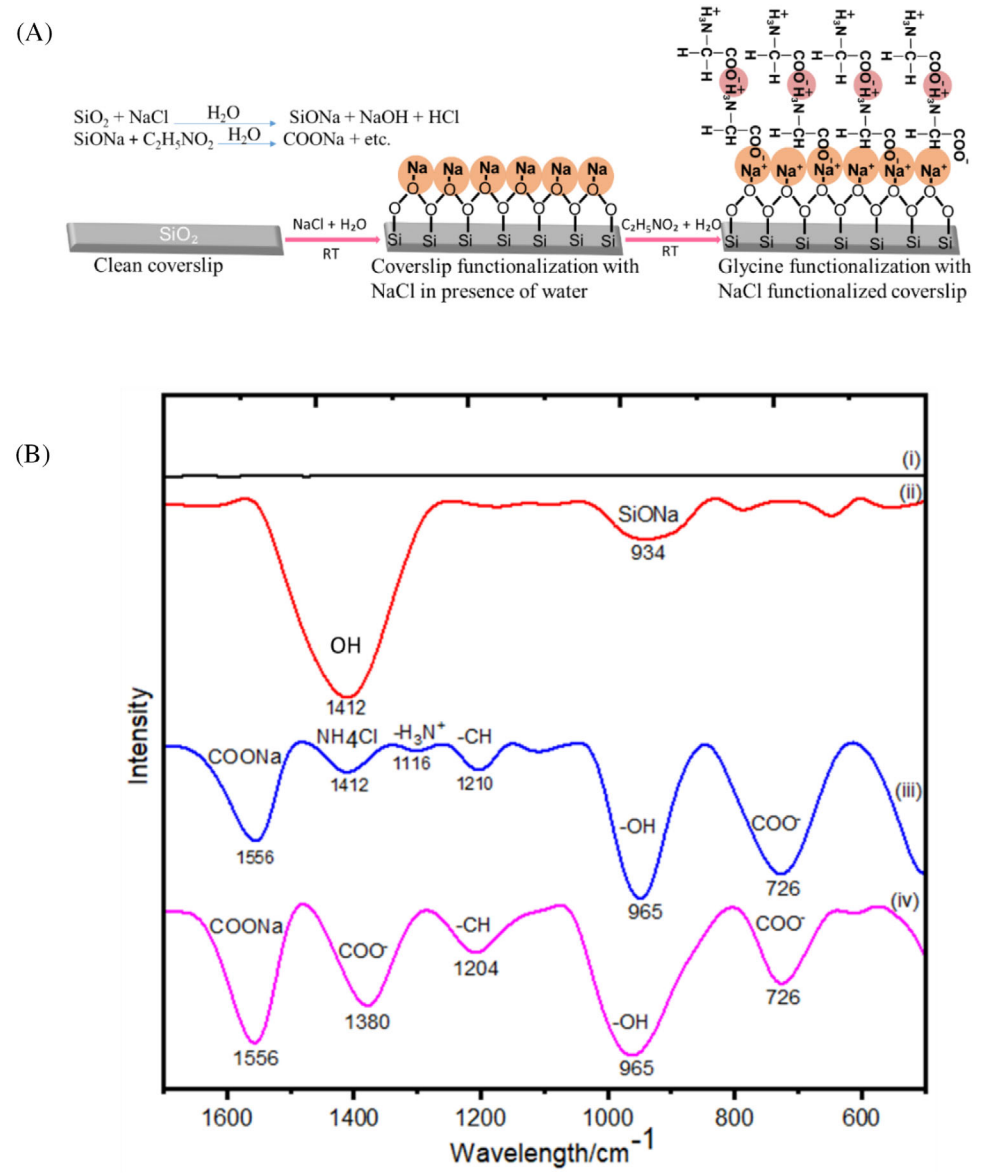

FIGURE 2 A, Schematically illustrated glycine functionalization steps and (B) FTIR analysis functionalization steps: (i) cleaned surface, (ii) NaCl treated surface, (iii) 6H glycine treated surface and (iv) 10H glycine treated surface

fabrication steps were investigated morphologically with AFM and SEM imaging while the Na^+ ionization (SiONa),[37] initiation glycine assembly (COONa) and glycine chain formation (NH_3^+:OOC^-) were confirmed with FTIR spectroscopy.

2.1 | Glycine functionalization on coverslip

The functionalization steps such as-establishment of Na^+ on a coverslip, initiation of glycine self-assembly and growth of glycine nanostructures were confirmed with FTIR, AFM and SEM investigations. The stretching of various functional groups formed during step-by-step functionalizations were measured using PerkinElmer FTIR in basic mode as illustrated in Figure 2A. The FTIR spectra revealed that significant changes occur at each glycine functionalization steps such as only cleaned glass slide appears no stretching[42] (Figure 2B i) whereas the spectra for NaCl treated coverslip showed clear stretching at 970 cm^{-1} and 1412 cm^{-1} for the formation of SiONa and NaOH (Figure 2B ii), respectively.[38,39,43,44] It is well known that in the presence of H_2O (aqueous solution) NaCl ionizes into Na^+ and Cl^- that Na^+ bonded with SiO_2 for the formation of SiONa (Figure 2B ii). Whereas the glycine functionalized surface showed distinct stretching at 1558 cm^{-1} for COONa vibration[38,40,45] while many other stretching 730, 965, 1116, 1202, and 1412 cm^{-1} appeared for COO^-, -CH, H_3N^+, -OH and NH_4Cl

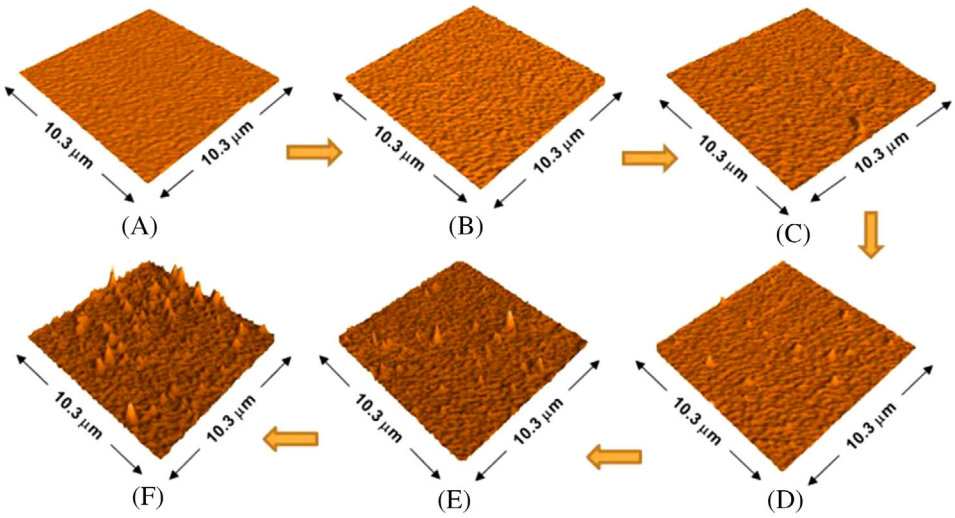

FIGURE 3 Three-dimensional view of AFM images of coverslip surfaces: (A) controlled (freshly cleaned coverslip), (B) 2H, (C) 4H, (D) 6H, (E) 8H and (F) 10H glycine treated surfaces

(Figure 2B iii and iv). This was because in the presence of water in glycine solution, SiONa ionized into SiO^- and Na^+, later the Na^+ bind with COO^- of glycine for the formation of COONa.[3,38–49] Thus FTIR spectra confirmed that glycine amino acid was established on coverslip through $SiONa^+$:COO^- covalent linkage while their anisotropic growth (glycine chain) appeared through H_3N^+:COO^- covalent linkage as shown in Figure 2A. Furthermore, the stability of those stretching's was determined from the FTIR spectra of prolonged periods (6H and 8H) of glycine exposed samples. The results revealed that most of the stretching remain stable except for shifting the stretching of NH_4Cl from1412 to 1380 cm^{-1} that represented COO^-[50–52] resulting (Figure 2B iv) from the denaturation of dissolve glycine amino acid in aqueous environment for prolonged exposure. However, the stability of stretching at 970, 1558, and 954 cm^{-1} that corresponds to SiONa, COONa and-OH group, respectively, revealed that self-assembled glycine is stable on the functionalized surface.

The nano-scale surface topography of the glycine functionalized coverslips was further investigated using topographic AFM images obtained with Nanosurf Flex AFM in contact mode from each step of the functionalization process as shown in Figure 3. The three dimensional (3D) AFM images of glycine functionalized coverslips for various period (ranging 2 to 10H) of glycine treatment were obtained for morphological investigations. The topographic images revealed a clear surface without forming of nanostructure for control (without glycine functionalized) and 2H glycine treated coverslip as shown in Figure 3A and 3B. Whereas there was a distinct growth of nanostructures appeared after 4H to 10H glycine treatment as shown in Figure 3C, 3D, 3E, and 3F. It was also revealed that the glycine nanostructures growth occurred anisotropically with the functionalization periods.[53]

The glycine functionalization steps were further verified by analyzing the topographic SEM images obtained from each step of the functionalization processes. The self-assembly of glycine nanostructure on a coverslip substrate for various periods of glycine treatment was illustrated in Figure 4. The results revealed that the growth of glycine nanostructures showed dependence on glycine treatment periods. The 0 and 2H exposure of glycine on coverslip yielded no growth of nanostructures as shown in Figure 4A and 4B while dots-like glycine nanostructures were revealed from ≥4H of exposure period as shown in Figure 4C-F. The morphological features of glycine nanostructures growth showed dependence on the exposure period. The dotted-like structure appeared upon 4H exposure, while such dotted structure showed further growth with the increasing periods of exposure. The elongated nanostructures with a mixture of dots were revealed from Figure 4D and 4E for 6H and 8H glycine treated samples while only elongated structures were obtained from 10H treated sample as illustrated in Figure 4F. These morphological features of various periods of glycine functionalized surface were completely coincident with that of AFM data. Thus, the time-dependent glycine growth on the coverslip was confirmed with both AFM and SEM investigations.

2.2 | Time-dependent growth of glycine nanostructures on coverslip

This time-dependent anisotropic glycine growth was further evaluated by analyzing and quantifying information of the height profile of AFM images. The Gaussian plot

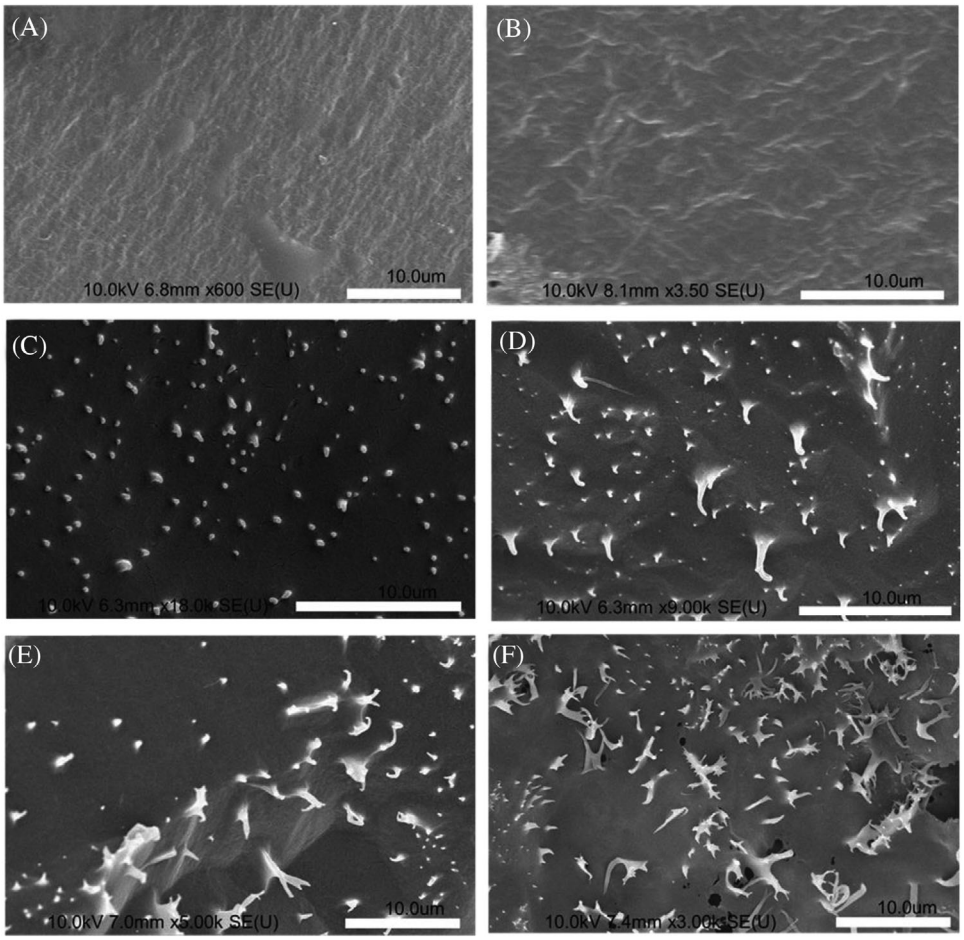

FIGURE 4 Scanning Electron Microscopic (SEM) images of coverslip surface: (A) controlled (freshly cleaned coverslip), (B) 2H, (C) 4H, (D) 6H, (E) 8H and (F) 10H glycine treated surfaces

derived from glycine nanostructure's density and height showed a time-dependent increase with the functionalization periods (2H, 4H, 6H, 8H, and 10H) as shown in Figure 5. The 2H functionalization sample showed 5–25 nm height with 0.063 nm^{-1} density (Figure 5A and 155 nm width (Figure S1) whereas at 4H, 6H, 8H, and 10H glycine functionalization samples showed 20–38, 55–83, 70–93, and 50–103 nm heights with 0.065, 0.039, 0.048, and 0.0243 nm^{-1} densities (Figure 5B-E), and 252, 300, 352, and 380 nm widths (Figure S2) respectively. The glycine growth curve derived from particle's height profile was shown in Figure 5, where the height increased with the increasing glycine treatment period. This time-dependent glycine growth on NaCl treated coverslip was initiated with the linkage between $SiONa^+$:COO^- that was revealed as a nanoscale dot arrangement as shown in Figure 3 and Figure 4 while with the course of time glycine formed chain-like structures throughout the surface using H_3N^+:COO^- bonding[39] as was revelled with FTIR vibration shown in Figure 2B iii and 2B iv. This glycine growth continued exponentially with glycine treatment period up to 8H whereas after 8H maximum vertical growth appears and this height was maintained steady-state up to 10H (Figure S2) indicating that maximum height of the glycine nanostructures was attained within 8H. At the same time, the widths and density of the nanostructures found to increase ≥6H post-treatment. Thus the 8H and 10H glycine treated samples showed numerous glycine nano to microstructures throughout the coverslip surfaces. Such glycine functionalized surfaces were supposed to provide sufficient adhesion motifs for BHK-21 cell adhesion and proliferation. Thus, the different periods of glycine treated coverslips were subjected to in vitro BHK-21 cell adhesion and proliferation assay to test this hypothesis.

2.3 | Adhesion strength assay of glycine functionalized surface

Various periods of glycine treated coverslips with different vertically and spatially grown nanostructures were subjected to BHK-21 cell adhesion study for determining their

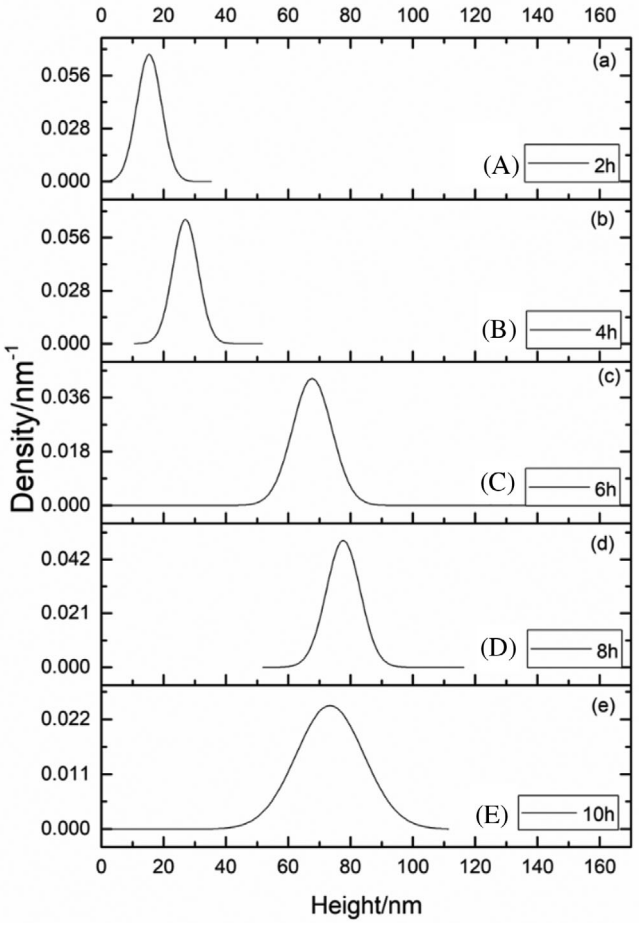

FIGURE 5 Gaussian curve derived from height profile analysis of AFM images: (A) 2H, (B) 4H, (C) 6H, (D) 8H and (E) 10H glycine treated surfaces

adhesion strength. The adhesion strength was determined employing shear stress as a means of matric compression forces applied on the micropipette during pipetting.[1,54,55] For this a total of 200 μL of cell suspension (0.4×10^3cell/chip) of BHK-21 cells were seeded on each freshly functionalized coverslip surface (Figure S4). The results of various shared force (pipetting time) were shown in Figure 6 revealing that adhesion strength increased with the glycine functionalization time (Figure 6A), this glycine functionalization time-dependent adhesion strength enhancement was noticed for all the shared force applied while the maximum adhesion strength revealed from 6.25 Pa pipetting and minimum was from 31.25 Pa which is because the number of erupted cells increased with periods of applied shared forces. Considering the highest adhesion strength, the adhesion performance of 10H glycine treated coverslip was further verified with a comparative study using RGD functionalized coverslip.[24,55] The results of the comparative adhesion strength of glycine and RGD functionalized coverslips were shown in Figure 6B. The adhesion strength of glycine and RGD treated BHK-21 cell immobilized coverslips showed non-significant differences (Figure 6B), while significant differences were noticed for the both when compared with control (non-functionalized) coverslips. These features of adhesion strength were observed for all the durations (6.25-31.25 Pa) of shared force application. Thus, the hypothesis of adhesion ability of glycine residues in adhesion peptides is proven.[24,53–55] Moreover, the glycine nanostructures modified surface found equally effective for establishing firm cell-substrate interactions as compared with a known potential synthetic adhesion peptides RGD.[1,53] Such adhesion ability of the glycine amino acids could be due to their interactions with cell surface receptor integrin as occurred during their association with RGD.[1] This integrin associated cell adhesion of glycine consisted of peptide derivatives was also proven elsewhere.[–2] Additionally, the glycine assisted modification of the hydrophobicity/surface charge of the glycine functionalized cover slip and the deposition of albumin could also be another basis adhesion mechanism. However, several studies on various vertically or horizontally aligned nanostructured RGD modified surfaces showed variations in adhesion performances (Kafi et al., 2012). Where the optimum adhesion performances were revealed only when the glycine residue of the RGD tripeptide sequence is aligned for the Integrin as shown in the Figure 1.[21–24] Thus along alignment or positioning of the glycine residue of the arginine-RGD tripeptide is critical for establishing firm adhesion process which is required for cell substrate interaction studies. Reason why, this study employed nanostructured glycine chain on the cover slip avoiding their crumbled appearances. Herein, the nanostructures formed with glycine chain acted as cell adhesion motifs throughout the functionalized surface to establish firm cell adhesion. Thus, the glycine nanostructure modified surfaces could be a suitable alternate to other adhesion protenis peptides and peptide derivates modified surface for establishing living cell on artificial surfaces.

2.4 | Effect of various glycine treatment period on BHK-21 cell proliferation

The various period of (2H to 10H) glycine treated coverslips were further subjected to BHK-21 cell proliferation for evaluating their proliferation efficiencies on different topographic glycine modified surfaces. For this a total of 200 μL of cell suspension (0.4×10^3cell/chip, Figure S4) were seeded on freshly functionalized coverslip surface. The growth morphology of BHK-21 cells on the functionalized surfaces were determined under a phase-contrast microscope (Figure 7), and results were illustrated in Figure 7A-E. The cell morphology and their growth pattern

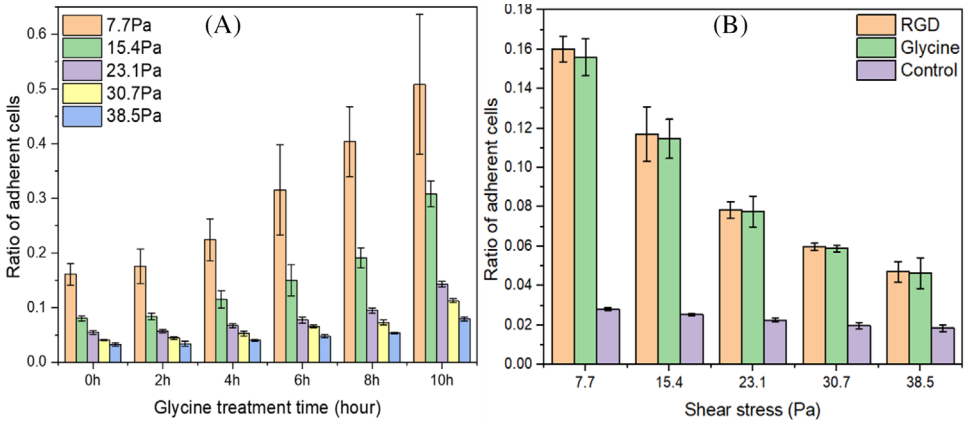

FIGURE 6 Adhesion strength assay of: (A) adhesion strength of glycine functionalization coverslip against various applied shared forces, (B) comparative adhesion performance of Glycine versus RGD peptides functionalized coverslips

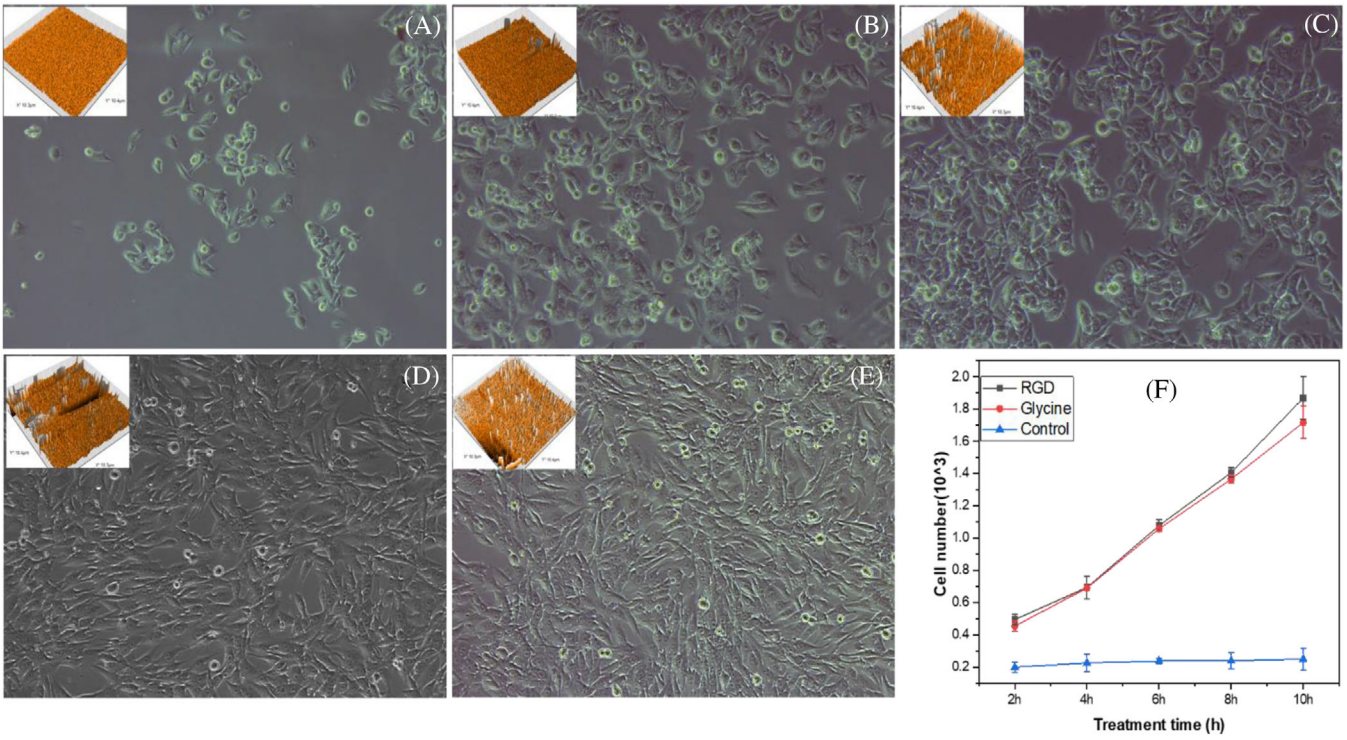

FIGURE 7 BHK-21 cell after 48H proliferation on 2H (A), 4H (B), 6H (C), 8H (DD) and 10H (E) glycine treated surfaces maintained in a standard cell culture incubator proving Dulbecco minimum essential medium supplemented with 1% antibiotic (100X) nutrient with 5% CO_2 and 70% humidity. F, The numbers of the cell from both the glycine and RGD treated surfaces together with nonrelated control. Inserted AFM images represent the respective surfaces on which cells were proliferated

showed strict dependence on the topographic patterns of glycine nanostructures established substrate where poor cell adhesion was achieved from 2 and 4H glycine treated substrate as shown in Figure 7A and 7B where a few cells were attached on the surface leaving the majority of the cell unattached and thus confluency was poor and ≤50% confluency was achieved from the 6H treated samples (Figure 7C). However maximum confluency (≥90%) in 8H glycine treated samples (Figure 7D) and 100% confluency was achieved from 10H Glycine treated samples (Figure 7E). Likewise, the Figure 7F showed glycine treatment time-dependent enhancement of cell proliferation for both the glycine and RGD treated surface with non-significant differences between them while there were significant

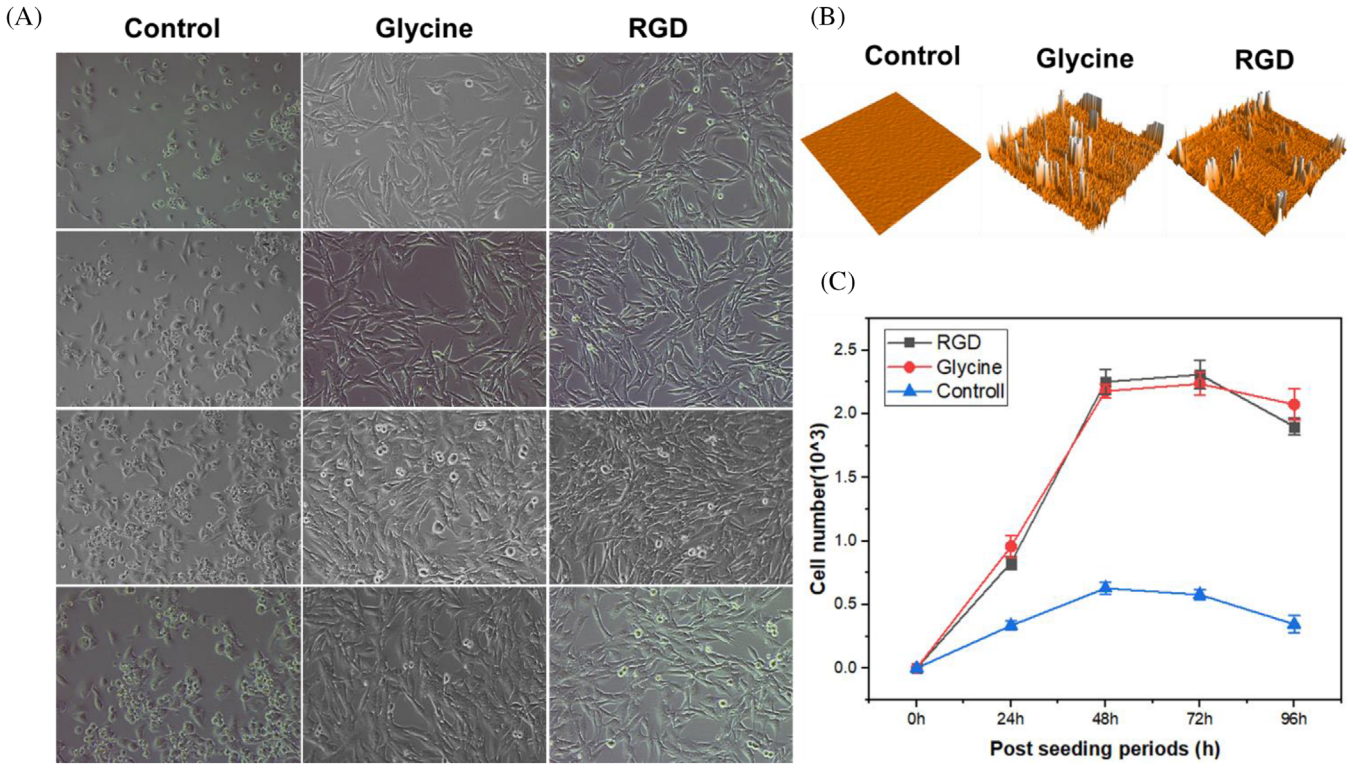

FIGURE 8 A, Comparative proliferations of BHK-21 cells on 10H glycine versus RGD peptide treated surfaces maintained for 24 to 96H in a standard cell culture incubator proving Dulbecco minimum essential medium supplemented with 1% antibiotic (100X) nutrient with 5% CO_2 and 70% humidity. B, AFM images of corresponding surfaces (control, glycine and RGD functionalized) on which proliferation performance were studied, (C) comparison of Growth curves of BHK-21 cell on glycine versus RGD peptide-functionalized surfaces derived from 0 to 96H post-seeding surfaces

differences with controlled (non-functionalized surface). Such proliferation tendencies of functionalized surfaces are obvious due to focal adhesion kinase (FAK) activation pathways.[1,53–55] Such RGD assisted FAK activation of the functionalized surface has been explored in our previous research[1,53] while enhancing cell proliferation on other AMs functionalized has been proven elsewhere.[2,3,5,7] It is well known that artificial surfaces modified with AMs offers firm adhesion followed by spreading and proliferation.[56] Here in the enhanced cell proliferation of glycine functionalized surface was achieved due to their firm focal adhesion[3,12–15] mediated cytoskeletal stretching[57] followed by cell division.[55] Thus the enhanced proliferation efficiency of glycine functionalized coverslip was proved.

2.5 | Matinance of BHK-21 cell on glycine functionalized surface for prolonged period

For investigating growth patterns on the glycine functionalized surface, batches of 10H glycine functionalized surface were subjected to BHK-21 cell seeding with equal (0.4×10^3cells/chip) concentration and allowed for several periods (24H to 96H) of culture and examined under a microscope for morphological investigations as well as cell counting at 24H interval and results are plotted in Figure 8. The glycine (middle column) and RGD (right column) treated surfaces did not show differences in confluences throughout the experimental periods while remarkable differences were shown with their corresponding control surfaces (left column). The morphological features of BHK-21 cells were shown in Figure 8A where the time-dependent enhanced confluences were found up to 48H as shown in middle and right column of Figure 8A whereas a confluent layer obtained after 48H of post-seeding and this was maintained up to 72H post-seeding. However, at 96H post-seeding the cells were bizarre shape with many apoptotic round cells which were erupted from both the functionalized surfaces. These features of growth were further confirmed with Trypan Blue based cell counting[24,55] from representative samples of each post seeding groups and results are illustrated in Figure 8B. The cell growth pattern showed an identical growth features of BHK-21 cells where cells were exponentially proliferated up to 48H and remained as a stationary phase from 48H to 72H followed by gradual decrease of cell numbers indicating the appearance of death phase

after 72H which was continued up to the last occasion of experimental period (96H). This was an ideal growth curve for any living cells as described elsewhere.[25] Thus, the glycine functionalized surface can be an ideal in vitro platform for many cell-based experimentations such as tissue engineering, biomedical engineering,[1] cell health monitoring,[2] drug effect study and so on.[,2]

3 | CONCLUSIONS

This research unveils cell adhesion and proliferation ability of glycine amino acid as an alternative of commonly practiced adhesion proteins, peptides and peptide derivatives. We have also demonstrated glycine functionalization strategies on artificial surface for enhancing baby hamster kidney (BHK-21) cell adhesion and proliferation. The glycine functionalization involves three basic steps such as (i) Na^+ ionization on coverslips, (ii) initiation of glycine assembly and (iii) elongation of glycine chain for yielding nanostructure. The Na^+ ionization is performed with rinsing the coverslips in NaCl solution for the formation of SiONa groups. The initiation of self-assembly is achieved through establishing $SiONa^+$:COO^- linkage using COO- groups of glycine. Whereas the elongation of glycine chain is achieved through H_3N^+:COO^- linkage between the H_3N^+ and COO^- groups of the two adjacent glycine molecules. This elongation of the glycine chain reveals various levels of nanostructures growth in a time-dependent manner. The chemical linkage appears during substrate functionalization process is confirmed by FTIR analysis while the formation of glycine nanostructures is investigated topographically with the AFM and SEM. The surface topographic investigation reveals that glycine nanostructure formation on coverslips increase anisotropically in a time-dependent manner. Thus, various period of glycine functionalized surfaces are subjected to BHK-21 cell adhesion and proliferation studies where the maximum cell adhesion is achieved from 10H functionalized surface. This 10H glycine functionalized surface is further used for comparing adhesion performance with conventionally practiced expensive RGD peptides revealing non-significant differences between them. Likewise, the proliferation performance of BHK-21 cells shows time-dependent enhancement throughout the experimental periods with non-significant differences between glycine and RGD functionalized surface while there are significant differences with the control for every occasion. Furthermore, the growth curve reveals from 0H-96H BHK-21 cell-cultured surface shows exponential growth phage for 0H-48H while a stationary growth phage appears between 48H and 72H followed by a phage of death is appeared up to 96H post-seeding. These features of growth curve shows non-significant differences between glycine and RGD functionalized surfaces while there are significant differences with control for both the functionalized surfaces. Thus, this research suggests that glycine amino acid is equally effective for establishing firm cell-surface interactions. This adhesion and proliferation ability of glycine holds primes for their use in the fields of tissue-engineering, cell biology, pharmacology, biomedical sciences, basic neuroscience and toxicology and so on, as an alternate of expensive adhesion proteins, peptides, and their derivatives.

4 | EXPERIMENTAL SECTION

4.1 | Chemicals and reagents

Glycine and PDMS were purchased from SIGMA-ALDRICH Co., St. Louis, USA. RGD peptides were purchased from Sigma-Aldrich St Louis, USA. BHK-21 (C-13, ATCC CCL-10) cell were parched from the Global Bioresource Center, American tissue culture collection (ATCC). Phosphate Buffered Saline, Trypsin, DMEM, Penicillin-Streptomycin (100X), HI FBS, were parched from Gibco, NY, USA. Pipette sets, TC Flasks, Serological Pipettes, Coverslip glasses, Hemocytometer and so on., were parched from Thermo Fisher Scientific, imported by Invitrogen Bioservices India Pvt. Ltd. Trypan blue were also parched from Calsson UT, USA. All chemicals and reagents were received and stored in laboratory repositories in safe and sound condition and used as required.

4.2 | Preparation of coverslip for glycine functionalization

Prior to glycine functionalization, the coverslips (Decglaser Cover Glass 22 × 22 mm) were cleaned thrice with HCl (37%) and Ethanol (70%) sequentially followed by flashing with Deionized Distrill Water (DDW) for removing biological contaminants and subsequently dried at room temperature (RT) under a dust proof clean environment.

4.3 | Step-by-step functionalization

Glycine amino acids were established on freshly cleaned coverslip through $SiONa^+$:OOC^- linkage. For this, at first, the freshly cleaned coverslip was deep in 0.1 M NaCl solution for 2H at RT for establishing SiO_2Na^+ where –Si = O group of coverslip covalently reacts with the Na^+ ion to

form SiONa compound as shown in the Figure 2A.[43,44,58] Secondly, the SiONa functionalized coverslip were subjected to 1 M glycine solution (in DDW) for various periods (2H, 4H, 6H, 8H and 10H) at 4°C for self-assembling of glycine nanostructures through COONa linkage[38,39,41,59] (Figure 2A). After treatment, glycine suspensions were decanted and washed with PBS and dried at RT. The glycine molecule consists of a basic amino (-NH_2) group and an acidic carboxylic (-COOH) group. Under neutral pH, there is an internal transfer of a hydrogen ion from the-COOH group to the-NH_2 group to leave the glycine molecule with both a negative charge and a positive charge and was termed as the zwitterion.[41] In a neutral solution glycine exists in a zwitterionic state with coexisting -NH_3^+ and -COO^- groups.[40] The glycine microstructures were formed through self-assembly of glycine molecules on NaCl treated coverslip surface. The onset of glycine self-assembly initiates when the COO^- group of zwitterionic glycine reacts with the available Na^+ group of the coverslip. With an increase in glycine exposure time, the chain self-assembly of glycine molecules occurs, which leads to the formation of glycine nanostructures on the surface of the coverslip that offered numerous adhesion motif for enhancing cell adhesion ability.

4.4 | RGD functionalization

RGD functionalized samples were prepared in parallel with glycine functionalization following the protocol described in our previous works[28,60] briefly commercially purchased RGD peptide from Sigma-Aldrich St Louis, USA and dissolved in PBS at a ratio of 1:99 and drop casted on the coverslip and incubated at 4°C for various period (2H, 4H, 6H 8H,10H) corresponding to glycine functionalization period. After functionalization the surface was cleaned aseptically and exposed to UV prior cell seeding experiment.

4.5 | Topographical investigation of functionalized surface

The topographical features of the glycine functionalized surfaces were analyzed with AFM and SEM. AFM was performed (Nanosurf FlexAFM) using contact mode to obtain the topographic features of the glycine functionalized surface. The dimensions of the nanostructures were measured from the height profile (Figure S1) of the topographic images. For SEM investigation of the surfaces was placed on the silicon wafer, and a thin layer of Au was sputtered on it prior to imaging. Images were obtained with a field emission scanning electron microscope (FESEM, Hitachi S-4700) at an accelerated voltage of 10 kV and 10 mA current. The step-by-step functionalization process was confirmed with the FTIR investigation. The samples were examined using an FTIR spectrometer (PerkinElmer FTIR) in basic mode (Golden Gate) using PerkinElmer IR spectroscopy software.

4.6 | Design and fabrication of PDMS chamber on glycine functionalized surface

We have particularly achieved a predesigned 2 × 2 cm^2 PDMS chip chamber (Figure S3) on glycine functionalized coverslip on which BHK-21 cell was established. The functionalized coverslip were evaluated for determining the effect of the glycine functionalization period on cell adhesion and proliferation and the growth pattern of BHK-21 cells on the chip over the post-seeding periods.

4.7 | Adhesion strength assay of the glycine functionalized surface

BHK-21 cells (at a concentration of 0.4 × 10^3 cell/chip) were seeded on the Glycine and RGD peptides functionalized coverslip and maintained at 37°C under 5% CO_2 atmosphere while BHK-21 cell-seeded freshly cleaned coverslip served as a control in parallel. At 24H post-seeding, the cell immobilized surfaces were subjected to adhesion strength assay as described elsewhere.[10,21,23,61] Briefly, the cultured medium was removed and a volume-controlled flow was employed by micropipette (10-200 uL) pumping with PBS for 6.25, 12,5, 18.25, 25 and 31.25 Pa, respectively. The erupted cells in PBS were subjected to Trypan blue exclusion assay.[62] Cell adhesion strength was determined by measuring the shear stress, as described in the previous report.[2,63] Briefly the shear stress (Pa) was measured using the equation as given below-

$$\tau = F/A \quad \text{(i)}$$

where τ = is the shear stress, F = is the force applied, A = is the area of chip, that is parallel to the force vector.

4.8 | Proliferation assay

BHK-21 cells were seeded at a definite density (Figure S4) (0.4 × 10^3 cell/chip) to the freshly prepared and aseptically cleaned surface. Then the seeded surfaces were incubated for 24H, 48H, 72H, and 96H for investigating cell proliferation and viability assay. Cell adhesion and confluences were confirmed with Microscopy using Inverted phase-contrast microscope (Primo Vert, Carl Zeiss

Microscopy GmnH 37081 Gottingen, Germany) while proliferation and viabilities were determined with Trypan Blue based cell counting method[61,64] with standard counting chambers under the microscope.

4.9 | Statistical analysis

All values expressed as mean ± standard deviation, and all experiments were repeated thrice. Data were analyzed using the computerized statistical program "Origin 8". Significant differences were determined for $^{**}p < 0.01$ and $^{*}p < 0.05$.

ACKNOWLEDGMENTS

This works is supported with Ministry of Education (MOE), Banbeis, (Project/User ID: LS2018687), Bangladesh and the International Science Program (ISP), Uppsala University, Sweden.

CONFLICT OF INTEREST

The authors declare no conflict of interest.

DATA AVAILABILITY STATEMENT

Research data are not shared.

ORCID

Md. Abdul Kafi https://orcid.org/0000-0001-8126-024X

REFERENCES

1. M. A. Kafi, T. H. Kim, C. H. Yea, H. Kim, J. W. Choi, *Biosens Bioelectron* **2010**, *26*, 1359.
2. M. A. Kafi, T. H. Kim, C. H. Yea, H. Kim, J. W. Choi, *Biotechnol Lett.* **2010**, *32*, 1797.
3. N. S. Kehr, K. Riehemann, J. El-Gindi, A. Schafer, H. Fuchs, H. J. Galla, L. De Cola, *Adv. Funct. Mater.* **2010**, *20*, 2248.
4. D. Pallarola, A. Bochen, H. Boehm, F. Rechenmacher, T. R. Sobahi, J. P. Spatz, H. Kessler. *Adv. Funct. Mater.* **2014**, *24*, 943.
5. X. Zhong, F. J. Rescorla, *Cell. Signal.* **2012**. *24*, 393.
6. B. T. Marshall, M. Long, J. W. Piper, T. Yago, R. P. McEver, Z. Cheng, *Nature* **2003**, *423*, 190.
7. J. A. Rowley, G. Madlambayan, D. J. Mooney, *Biomaterials*. **1999**, *20*, 45.
8. A. J. Garcia, M. D. Vega, D. Boettiger, *Mol. Biol. Cell*. **1999**, *10*, 785.
9. T. Groth, G. Altankov, A. Kostadinova, N. Krasteva, W. Albrecht, D. Paul, *J Biomed. Mater. Res.* **1999**, *44*, 341.
10. L. Tang, Y. Wu, R. B. Timmons, *J Biomed Mater Res*. **1998**, *42*, 156.
11. L. Bačáková, E. Filová, F. Rypáček, V. Švorčík, V. Stary, *Physiol Res.* **2004**, *53*, S35.
12. M. A. Kafi, A. Paul, A. Vilouras, R. Dahiya, *Biosens Bioelectron.* **2019**, *147*, 19–02308.
13. N. Huettner, T. R. Dargaville, A. Forget, *Rends Biotechnol.* **2018**, *36*, 4.
14. R. Fujisawa, M. Mizun, Y. Nodasakat, Y. Kuboki, *Matrix Biol.* **1997**, *16*, 21.
15. J. Conradi, S. Huber, K. Gaus, F. Mertink, S. R. Gracia, U. Strijowski, S. Backert, N. Sewald, *Amino Acids*. **2012**, *43*:219.
16. K. Ramaker, M. Henkel, T. Krause, N. Röckendorf, A. Frey, *Drug Deliv.* **2018**, *25*, 928.
17. S. Soylemez, B. Demir, G. O. Eyrilmez, S. Kesici, A. Saylam, D. O. Demirkol, S. Ozçubukçu, S. Timur, L. Toppare, *RSC Adv.* **2016**, *6*, 2695.
18. S. L. Bellis, *Biomaterials* **2011**, *32*, 4205.
19. H. B. Lin, C. G. Echeverria, S. Asakura, W. Sun, D. F. Masher, L. C. Stuart, *Biomaterials* **1992**, *13*, 905.
20. K. P. Walluscheck, G. Steinhoff, S. Kelm, A. Haverich, *Eur. J. Vasc. Endovasc. Surg.* **1996**, *12*, 321.
21. N. Huettner, T.R. Dargaville, A. Forget, *Trends Biotechnol.* **2018**, *36*, 4.
22. M. A. Kafi, H. Y. Cho, J. W. Choi, *Nanomaterials*. **2015**, *5*, 1181.
23. T.G. Kapp, F. Rechenmacher, S. Neubauer, O,V. Maltsev, E.A. Cavalcanti-Adam, R. Zarka, U. Reuning, j. Notni, H.J. Wester, C. Mas-moruno, J. Spatz, B. Geiger, H. Kessler, *Sci Rep.* **2017**, *7*, 39805.
24. M. A. Kafi, M. K. Aktar, Y. Phanny, M. Todo, R. Dahiya, *Regen. Biomater.* **2019**, *7*, 1.
25. M. A. Kafi, H. Y. Cho, J. W. Choi, *Nano Converg.* **2016**, *3*, 17.
26. M. A. Kafi, A. Paul, A. Vilouras, R. Dahiya, *Biosens. Bioelectron.* **2020**, *147*, 11781.
27. A. D. Theocharis, S. S. Skandalis, C. Gialeli, N. K. Karamanos, *Adv. Drug Deliv.* **2015**, *97*, 4.
28. M. A. Kafi, W. A. El-Saida, T. H. Kim, J. W. Choi, *Biomaterials.* **2012**, *33*, 731.
29. D. L. Kusindarta, H. Wihadmadyatami, *Tissue Regeneration*. (Eds: M. W. King) IntechOpen, London, UK **2018**, The Role of Extracellular Matrix in Tissue Regeneration 65. https://doi.org/10.5772/intechopen.75728.
30. M. Meyer, *Biomed. Eng.* **2019**, *18*, 1.
31. A. Sorushanova, L. M. Delgado, Z. Wu, N. Shologu, A. Kshirsagar, R. Raghunath, M. A. Mullen, Y. Bayon, A. Pandit, M. Raghunath, *Adv. Mater.* **2019**, *31*, 1.
32. A. L. Fidler, S. P. Boudko, A. Rokas, B. G. Hudson, *J. Cell Sci.* **2018**, *10*, 131.
33. K. Rubin, M. Hook, B. Obrink, R. Timpl, *J. Cell Biol.* **1981**, *24*, 463.
34. G. Cynthia, J. Daniel, L. Sandra, B. James, B. Gregg, *J. Biol. Chem.* **1993**, *268*, 14153.
35. G. L. Richard, A. Kyriacos, *Tissue Eng.* **2000**, *6*, 85.
36. C. Dong, Y. Lv, *Polymers* **2016**, *8*, 42.
37. P. J. Babu, R. K. Alla, V. R. Alluri, S. R. Datla, A. Konakanchi, *Am. J. Mater. Sci.* **2015**, *3*, 13.
38. P. B. Capstick, R. C. Telling, W. G. Chapman, D. L. Stewart, *Nature* **1962**, *195*, 1163.
39. D. H. Lee, R. A. Condrate Sr., W. C. Lacoursenys, *J. Mater. Sci.* **2000**, *35*, 4961.
40. M. M. B. Keßler, H. J. Adler, K. Lunkwitz, *Macromol. Symp.* **2004**, *210*, 157.
41. R. G. Laughlin, *Langmuir* **1991**, *7*, 842.
42. N. Abidi, P. Aminayi, L. Cabrales, E. Hequet *ACS Symp. Ser.* **2012**, *1107*, 149.
43. H. S. Park, J. S. Lee, J. Han, S. Park, J. Park, *Energies.* **2015**, *8*, 8704.
44. J. G. Gwon, S. Y. Lee, G. H. Doh, J. H. Kim, *J. Appl. Polym. Sci.* **2010,**116, 3212.
45. K. W. Evanson, M. W. Urban, *J. Appl. Polym. Sci.* **1991** *42*, 2287.

46. U. A. Nagy, H. I. Lacko, B. F. Devínsky, L. Krasnec, *Chem. Zvesti.* **1976**, *30*, 541.
47. R. Liu, H. Lu, L. Wang, M. Tian, W. Sun, *Minerals* **2019**, *9*, 41.
48. R. A. Kumar, R. E. Vizhi, N. Sivakumar, N. Vijayanb, D. R. Babua, *Int. J. Light Electron Opt.* **2011**, *5*, 51592.
49. S. Suresh, A. Ramanand, D. Jayaraman, S. M. N. Priya, K. Anand, *Int. J. Phys. Sci.* **2011**, *6*, 3875,
50. A. Ramedania, A. Yazdanpanahb, A. Abrishamkarc, M. Nasrollahib, P. B. Miland, Z. H. Moghadame, N. P. S. Chauhanf, F. Sefatg, M. Mozafarid, *Advanced characterization tools for PANI and PANI-clay nanocomposites*. Elsevier Inc, Amsterdam **2019**, Ch 12.
51. A. Tinti, V. Tugnoli, S. Bonora, O. Francioso. *J. Cent. Eur. Agric.* **2015**, *16*, 1.
52. B. Y. G. Onak, B. Yurtseven, O. Gökmen, O. Karaman, *Comparison of the Effect of RGD Peptide Conjugation on Titanium Discs with Different Methods on Cell Adhesion and Proliferation*, Vol. 1, IEEE, Magusa, Cyprus **2018**, 16978-1-5090-2386-8.TIPTEKNO'18.
53. P. R. Sajanlal, T. S. Sreeprasad, A. K. Samal, T. Pradeep, *Nano Rep.* **2011**, *2*, 883.
54. A. Sigal, D. A. Bleijs, V. Grabovsky, S. J. V. Vliet, O. Dwir, C. G. Figdor, Y. V. Kooyk, R. Alon, *J. Immunol.* **2000**, *165*, 442.
55. M. A. Kafi, M. K. Aktar, Y. Phanny, M. Todo, *J. Mater. Sci. Mater. Med.* **2019**, *30*, 131.
56. J. Wegener, A. J. H. Galla, *Eur. Biophys. J.* **1998**, *28*, 26.
57. P. Sacco, G. Baj, F. Asaro, E. Marsich, I. Donati, *Adv. Funct. Mater.* **2020**, *30*, 2001977.
58. M. F Vieira, A. M. S Vieira, G. M Zanin, P. W Tardioli, C. M. J. M Guisán, *J. Mol. Catal. B Enzym.* **2011**, *69*, 47.
59. C. Caviglia, K. Zór, S. Canepa, M. Carminati, L. B. Larsen, R. Raiteri, T. L. Andresen, A. Heiskanen, J. Emnéus, *Analyst* **2015**, *140*, 3623.
60. M. A. Kafi, H. Y. Cho, J. W. Choi, *Nanomater* **2015**, *5*, 1181.
61. K. V. Vijayan, P. J. Goldschmidt-Clermont, C. Roos, P. F. Bray, *J. Clin. Invest.* **2000**, *105*, 793.
62. *Fundamental Techniques in Cell Culture*, 4th Edition. Laboratory Handbook, MRECK Darmstadt, Germany **2017**.
63. K. V. Vijayan, T. C. Huang, Y. Liu, A. Bernardo, J. F. Dong, P. J. Goldschmidt-Clermont, B. R. Alevriadou, P. F. Bray, *FEBS. Lett.* **2003**, *540*, 41.
64. O. A. Kofanova, K. Davis, B. Glazer, Y. De Souza, J. Kessler, F. Betsou, *Biopreserv Biobank*. **2013**, *12*, 206.

AUTHOR BIOGRAPHIES

Aminur Rahman is a Masters of Science student in the Department of Microbiology and Hygiene at Bangladesh Agricultural University, Mymensingh-2202. He received his BSc degree in microbiology from Jessore University of Science and Technology. Currently He is working on "development of BHK-21 cell based chip for electrochemical detection of FMD virus infection" as MS fellow at Nano-Biomaterial Engineering Lab (NBEL) group under the supervision of Md. Abdul Kafi. His current research interest includes nanotechnology, tissue engineering, biosensor and biomaterials.

Kumar Jyotirmoy Roy, a Doctor of Veterinary Medicine (DVM) graduate from Bangladesh Agricultural University (2013-2017). He has completed his post-graduation from the same university in microbiology (Jan, 2018-June, 2019). He worked on state-of-the-art techniques for bacteria isolation and identification and antibacterial activity using nanoparticles that characterized by Atomic Force Microscopy (AFM) for his experiment during post-graduation on Nano-Biomaterial Engineering Lab (NBEL). Currently he is working on cell chip design and fabrication for rapid, label-free detection of various infections through electrochemical investigation at same group under supervision of Md. Abdul Kafi.

Md. Abdul Kafi received DVM and MS in microbiology from BAU, Bangladesh. He pursued his PhD from Sogang University, Korea. He was awarded with Japanese Society for the Promotion of Science (JSPS) fellowship for working at Kyushu University, Japan. He also worked as a Marie Curie Individual fellow at University of Glasgow, UK. He has been working on cell-subtrate interaction studies since 2007 and achieved significant skills on bionanotechnology for developing cell based chip, invitro tissue engineering and Biosensors. Now, he is leading Nano-Biomaterial Engineering Lab (NBEL) for developing cell-based sensor, biodresorbable platform for wearables/implantables and intro tissue regenaration.

SUPPORTING INFORMATION

Additional supporting information may be found online in the Supporting Information section at the end of the article.

How to cite this article: A. Rahman, K. J. Roy, K. M. A. Rahman, M. K. Aktar, M. A. Kafi, M. S. Islam, M. B. Rahman, M. R. Islam, K. S. Hossain, M. M. Rahman, H. Heidari, *Nano Select* **2022**, *3*, 188. https://doi.org/10.1002/nano.202100043